A Marie-Curie-ITN within H2020

migrate microfluidics

ISTEGIM 2019

Proceedings of the International Symposium on Thermal Effects in Gas flows In Microscale October 24-25, 2019 – Ettlingen, Germany

ISTEGIM 2019 - 283392

QUANTIFYING ENHANCED INTERFACIAL THERMAL CONDUCTANCE AT SOLID-FLUOROCARBON LIQUID INTERFACES MODIFIED WITH SELF ASSEMBLED MONOLAYERS

Philip Darragh*[,1,2], Kenny Yu*[,1,3], Michael Morris[2], David McCloskey[3], Ryan Enright[1,†]

*These authors contributed equally

[1]Thermal Management Research Group, Efficient Energy Transfer (ηET) Department, Nokia Bell Labs, Dublin 15, Ireland

[2]AMBER Research Centre and School of Chemistry, Trinity College Dublin, Dublin 2, Ireland

[3]AMBER Research Centre and School of Physics, Trinity College Dublin, Dublin 2, Ireland

[†]ryan.enright@nokia-bell-labs.com

KEY WORDS

Heat transport, interface conductance, optical thermal metrology, FDTR, polymer thin-film, SAM, thiol chemistry, solid liquid thermal interface conductance.

ABSTRACT

As electronic and optoelectronic systems become increasingly miniaturized and integrated, local heat source densities are increasing. In this context, the role of interfaces becomes increasingly important in defining the performance of small scale heat exchangers providing thermal management. In particular, a thermal boundary resistance manifests at a solid-liquid interface as a result of a mismatch in vibrational spectra between the solid and liquid. This interface resistance is relevant to the performance of both intensive single- and two-phase fluidic thermal management implementations. Similar to the temperature jump observed at solid-gas and liquid-gas interfaces, the solid-liquid interface resistance/conductance impedes/promotes the flow of thermal energy. Thus, quantifying this interface property and identifying strategies to enhance it is paramount to the development of future high-performance heat exchangers. Here we used frequency-domain thermoreflectance to measure the interface thermal properties of gold in contact with water, ethanol and a model fluorocarbon heat transfer fluid, Galden HT80. Thiolated self-assembled monolayers were introduced onto the gold surface to study their effect on the interface thermal transport characteristics of the selected working liquids. Our measurements confirmed that self-assembled monolayers can enhance interfacial thermal conductance in the case of water and ethanol and suggest that Galden HT80 has a thermal interface conductance ~100× smaller than water. However, current limitations in our thermal metrology technique precluded us from confirming that self-assembled monolayers can enhance the interface conductance of Galden HT80 in contact with gold.

1. INTRODUCTION

In two-phase cooling, the latent heat of vaporisation allows thermal energy to be removed from the system at very high rates. However, the performance of two-phase exchangers are often limited by the thermal conductivity κ of the working fluid and the surrounding solid limiting the ultimately achievable heat transfer rate. Typically neglected in macroscopic heat exchangers, interfacial resistances become significant or even dominating in state-of-the-art two-phase heat exchanger concepts [1]. In particular, the coupling of heat from the solid to the liquid as it flows to the liquid-vapor interface has received little attention in the context of such systems. Recent work investigating the thermal properties of the solid-liquid interface has focused on modifying the solid-liquid interface to improve thermal conductance [2]–[6]. The use of self-assembled

monolayers (SAMs) to tailor the interfacial thermal conductance *G* through modification of the van der Waals interaction strength at solid-liquid interfaces has been demonstrated. Additional molecular layers bound to a metal interface have been shown to increase and decrease thermal resistances depending on the chemical nature of the terminal end group. Multiple studies have been carried out to modify the interfacial energy of surfaces through self-assembled monolayers (SAMs) [2],[7],[4].

Time domain thermoreflectance (TDTR) measurements have been carried out with various SAMs of differing functional groups [3]. It was found that hydrophilic end groups exhibiting strong specific interactions with polar solvents such as water can enhance the thermal interface conductance. Ge *et al.* have estimated a *G* value of ~100 $MWm^{-2}K^{-1}$ for the Au-water interface with a hydrophilic SAM produced from adsorption of 11-mercapto-1-undecanol ($C_{11}H_{24}$-OH ligand) [2]. Using TDTR, Harikrishna *et al.* showed that *G* is proportional to the thermodynamic work of adhesion between gold and water for a series of five alkane-thiol monolayers at the gold-water interface [3]. They were able to achieve $G = 190 \pm 30$ $MWm^{-2}K^{-1}$ for Au-water with a hydrophilic 11-mercapto-undecanoic acid (COOH). However, it remains unclear what impact SAMs will have on *G* in systems demonstrating non-specific interactions, e.g., fluorinated SAM in contact with a fluorocarbon liquid. Moreover, it appears that interface conductance's for this class of important dielectric heat transfer liquids have not been characterized.

In this paper, we synthesized and characterize SAMs assembled on the surface of Au using contact angle goniometry and atomic force microscopy (AFM). Using frequency-domain thermoreflectance (FDTR) [8], we explored the effect on *G* of gold-supported hydrogenated and fluorinated SAMs in contact with liquid water, ethanol and the perfluoropolyether, Galden HT80. Gold was chosen as it provides desirable thermoreflectance characteristics for our laser setup in addition to being relatively inert, having low oxophilicity (will not form an oxide in ambient conditions) and can readily facilitate the formation of well-ordered SAMs.

2. EXPERIMENTAL

2.1 Materials

The materials used in this work were, 1-decanethiol (96%) $CH_3(CH_2)_9SH$ and *1H,1H,2H,2H*-Perfluorodecanethiol (97%), CF_3 $(CF_2)7CH_2CH_2SH$ were purchased from Sigma Aldrich. Both SAM molecules are C_{10}. The simple structure diagrams of these two thiol molecules is shown in Figure 1. High performance liquid chromatography (HPLC) grade deionised water, IPA (for washing glass substrate before Au deposition) and ethanol were also bought from Sigma Aldrich. Galden HT80 was obtained from Solvay Specialty Polymers Italy S.p.A.

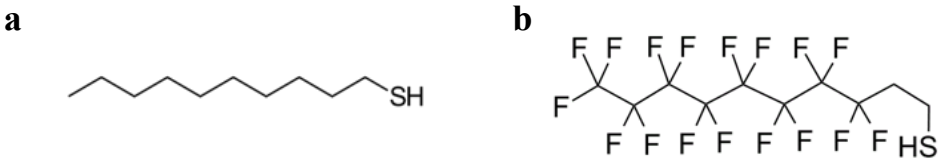

Figure 1. Simple structure diagrams of the investigated thiolated SAMs: **(a)** 1-decanethiol (1DT) **(b)** *1H,1H,2H,2H*-perfluorodecanethiol (PFDT)

2.2 Fabrication

As shown schematically in Figure 2, a thiol chemistry is implemented on an Au-coated glass substrate which doubles as the sensor layer for our thermal measurements. Alkylated thiols can be adhered to the Au surface through a chemical self-assembly process. The SAM layers are composed of three main parts; the active thiol head group, the carbon back bone and the functionalised end group. Chemisorption is driven by the soft sulphur ligand having favourable interaction with the Au atoms indicated by HSAB theory. The mechanism of adhesion to Au is still unclear, however several mechanisms have been proposed by Ulman *et*

al [11]. Firstly, the removal of the H atom from the thiol active group results in the generation of H_2. Additionally, these H atoms are generated from the metal hydrides on the surface of the metal at surfaces where the SAM layers have not been bound. Finally, the side products that can generate from the reaction may also produce hydrogen peroxide and water. Ulman thermodynamically calculated that the overall free energy of the exothermic adsorption process to be -5 kcal mol^{-1}, identifying the reaction as spontaneous at room temperature. Thiolated SAMs can be easily formed on the Au surface *via* self-assembly from solution [7]. Characterization of the untreated gold surface and synthesized SAM layers was performed using contact angle measurements to define the surface energy [12] of each surface and atomic force microscopy (AFM) to determine surface uniformity at microscopic dimensions.

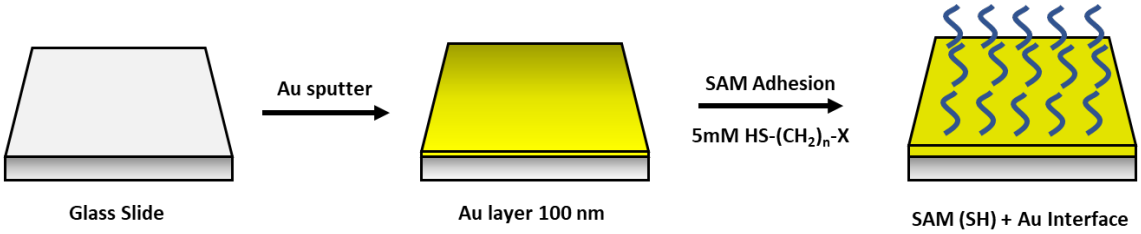

Figure 2. Process steps for adhesion of SAM to gold sensor surface

Glass substrates (SiO_2) with native oxide was cleaved into 1x1" pieces and degreased by sonication using IPA for 20 mins. Physiosorbed impurities on the substrate was removed by oxygen plasma before deposition. 2 nm of Ti adhesion layer followed by 100 nm of Au was deposited on to substrate using a Temescal vapor deposition tool. Substrates were firstly washed in ethanol followed by a vertical immersion into a 5 mmol thiol ethanolic solution (**a.** 1-decane thiol (1DT), **b.** *1H, 1H, 2H, 2H* Perfluorodecanethiol (PFDT)) that was left overnight at room temperature. Samples were then sonicated in ethanol for 10 minutes to terminate self-assembly followed by a N_2 blow. Samples were stored in desiccator to minimise contamination prior to FDTR analysis. Gold coated glass samples were used as a standard to compare the difference in the thermos-properties between the SAM layers and the substrate.

2.3 Surface characterisation

Characterization of the untreated gold surface and synthesized SAM layers was performed using contact angle measurements to define the surface energy [12] of each surface and atomic force microscopy (AFM) to determine surface uniformity at microscopic dimensions.Dynamic contact angle (CA) measurements were recorded for each sample using a high speed camera (60 Hz sampling rate) to capture advancing and receding CAs of two probe liquids (water and diiodomethane). Liquids were dispensed at a flow rate of 6 nLs^{-1} using a 35-gauge needle (135 µm OD) with a droplet volume of 60 – 90 nL. Surface energy analysis was determined from the advancing CA's of the two probe liquids using the Fowkes approach [13], [14]. Measurements were carried out on three samples for each different surface characterisation. Atomic force microscopy (AFM) were performed using a Park Systems XE7 with a non-contact mode cantilever (PPP-NCHR) with a force constant of ~42 Nm^{-1} and a resonant frequency of ~ 300 kHz. The AFM probe tip radius was ~7 nm.

2.4 FDTR thermal measurements

Frequency domain thermoreflectance (FDTR) is a non-contact optical metrology technique and is a derivative of the more commonly known time-domain thermoreflectance (TDTR) technique. Both techniques are widely used for measuring κ and G [8]. We have chosen FDTR over TDTR as it has proven to be a viable technique in measuring thermal properties of thin film while not needing to deal with the mechanical stage problem in TDTR [15]. More recently, FDTR has been used to measure solid-liquid interfaces for thermal applications.[16] Our FDTR setup is based on a pump and probe principle, with essential components shown in Fig. 2 [16].

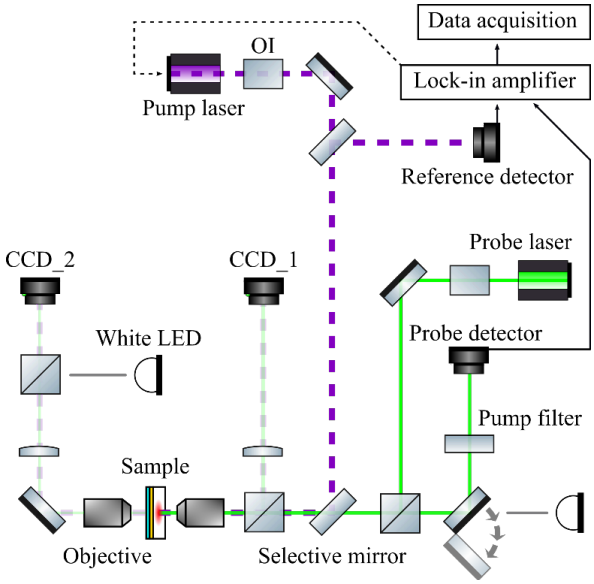

Figure 3. A schematic of the FDTR setup used in this work, inspired by Schmidt *et al.*[8]

Since our samples have a stacked layered configuration (see Fig. 3 (a)), we used a multi-layered bidirectional heat transfer model (see Fig. 3 (b)) to solve the inverse heat transfer problem to extract the quantities of interest, namely the liquid κ and the fluid/substrate interface G [17].

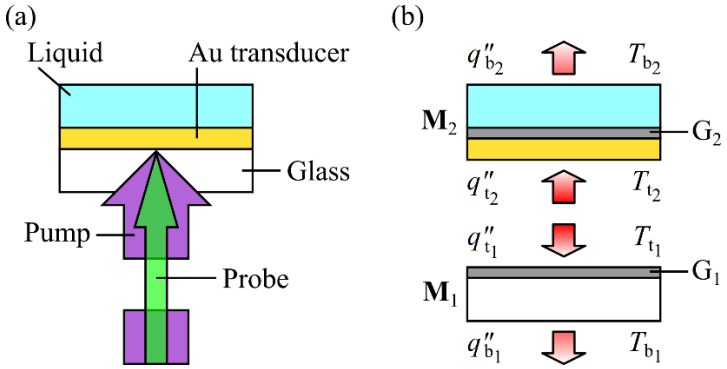

Figure 4. Schematic of (a) sample structure with indication of incident pump and probe beam direction, and (b) bidirectional heat flow problem separated into simpler and smaller multiple unidirectional heat flow problems [16].

For conduction heat transfer, Carslaw and Jaeger [18] described the heat transfer response $h(r,\omega)$ in a semi-infinite solid heated on its surface by a periodic point heat source as

$$h(r,\omega) = \frac{\exp(-qr)}{2\pi\kappa_r r}, \qquad q^2 = \frac{i\omega C_v}{\kappa_r}, \tag{1}$$

where r is the radial distance in the sample from the point heat source, ω is the angular frequency, κ_r is the radial thermal conductivity and C_v is the volumetric heat capacity of the sample. Our sample can be considered as to be composed of n layers, the top and bottom temperature T_t, T_b and heat flux q''_t, q''_b of the individual layer, and the nature of their interfaces influence the heat propagation can be related by the transfer matrix [18]

$$\begin{bmatrix} T_b \\ q''_b \end{bmatrix} = \prod_{i=n}^{1} \mathbf{M}_i \begin{bmatrix} T_t \\ q''_t \end{bmatrix} = \begin{bmatrix} A & B \\ C & D \end{bmatrix} \begin{bmatrix} T_t \\ q''_t \end{bmatrix}, \tag{2}$$

where $\mathbf{M}_i$ is defined as [18]

$$\mathbf{M}_i = \begin{bmatrix} \cosh(q_{r_i} d_i) & \dfrac{-\sinh(q_{r_i} d_i)}{q_{r_i}\kappa_{z_i}} \\ -q_{r_i}\kappa_{z_i}\sinh(q_{r_i} d_i) & \cosh(q_{r_i} d_i) \end{bmatrix}, \qquad q^2 = i\frac{\omega}{\alpha} \tag{3}$$

where d_i is the thickness of the i^{th} layer, κ_z is the cross-plane thermal conductivity, α is the thermal diffusivity and $\mathbf{M}_n$ is the matrix of the most bottom layer. For an interface, the thermal interface conductance G is defined by

$$q'' = G(T_1 - T_2). \tag{4}$$

Using the bidirectional approach, the temperature of the Au layer at the Au-glass interface can be rewritten form the top temperature expression [17]

$$T_t = \frac{-D}{C} q''_t \quad \rightarrow \quad T = \left(\frac{-D_1 D_2}{D_1 C_2 + D_2 C_1}\right) q''. \tag{5}$$

The cylindrical symmetrical problem can be solved by applying the Hankel transform. Taking the inverse Hankel transform gives a frequency response H for bidirectional heat transfer

$$H(\omega) = \mathrm{C} \int_0^\infty \left(\frac{-D_1 D_2}{D_1 C_2 + D_2 C_1}\right) \exp\left(\frac{\pi^2 k^2 (w_1^2 + w_2^2)}{2}\right) k dk, \qquad \mathrm{C} = \frac{\pi a \kappa_{TR} w_1 w_2 P_1 P_2}{2}, \tag{6}$$

where k is the transform variable, a is the absorption coefficient, κ_{TR} is the thermoreflectance coefficient of the transducer and w_1 and w_2 are the pump and probe spot radius while P_1 and P_2 are the pump and probe powers, respectively [17].

2.5 FDTR liquid measurement cell

Liquid cells were constructed to test the various samples with each individual working fluid in our FDTR setup. The fluids were encapsulated within the volume generated by a compatible o-ring sandwiched between the sample and a glass window. As can be seen in **Figure 5**, by incorporating the glass window, this cell setup allowed us to monitor the surface visually through the liquid using a 10× objective and a second CCD camera (see Figure 4, CCD_2).

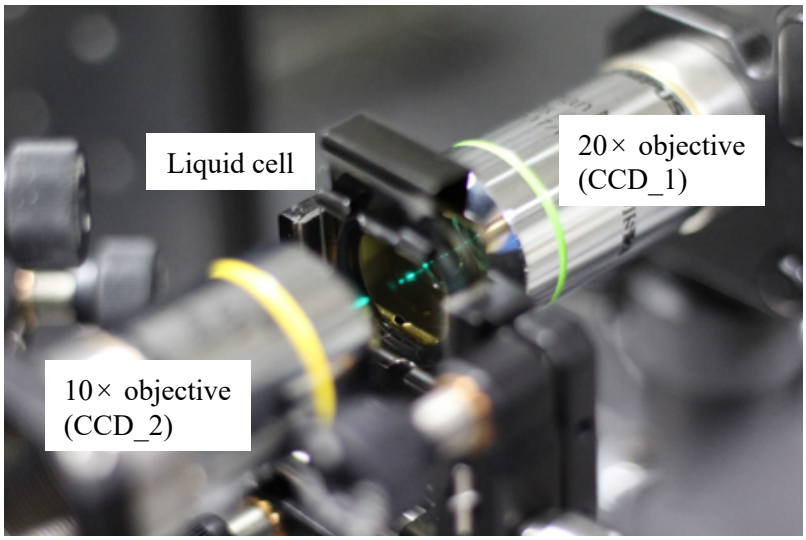

Figure 5. Image of the liquid cell installed in the beam line of the FDTR setup.

3. RESULTS & DISCUSSION

3.1 Contact angle measurements

Contact angle measurements were carried out using the infuse/withdraw method on bare gold surfaces and both SAM species assembled on the gold surface to quantify surface wetting characteristics as shown in Figure 6. To ascertain the surface energy contributions of the surfaces, deionised water (strongly polar) and

diiodomethane (weakly polar) were used as probe liquids. Advancing (θ_a) and receding (θ_r) contact angles between the surface and the probe liquid were measured at the three-phase contact line of the droplet using Image J software [19]. Contact angle hysteresis, e.g., the difference between the advancing and receding contact angles ($\Delta\theta = \theta_a - \theta_r$) can arise from surface roughness and chemical heterogeneity effects, though θ_a is expected to encode relevant information regarding the nominal chemical nature of surface[20]. Thus, the measured θ_a were used to determine the surface energy contributions estimated using the Fowkes method [13], [14] and the known polar/dispersive properties of the probe liquids by:

$$\sigma_{ls} = \sigma_{lv} + \sigma_{sv} - 2\left(\sqrt{\sigma_{lv}^{D}.\sigma_{sv}^{D}} + \sqrt{\sigma_{lv}^{P}.\sigma_{sv}^{P}}\right), \quad (7)$$

where σ is the excess surface energy between the liquid (l), solid (s) and vapor (v) with superscripts D and P interpreted as the dispersive and polar contributions, respectively.

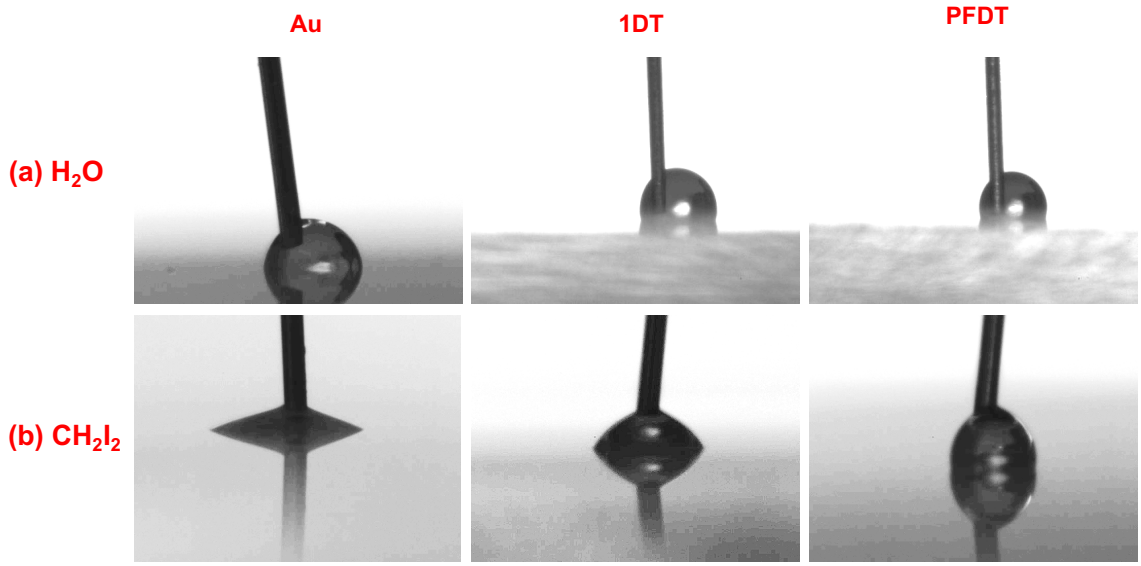

Figure 6. Advancing contact angle images for (a) water and (b) diiodomethane for bare gold (Au), 1-decane thiol (1DT) and *1H,1H,2H,2H*-perfluorodecanethiol (PFDT). For scale reference, the dispensing needle has an outer diameter of 135 µm.

Figure 7a identified that PFDT has the highest advancing contact angle ($\theta_a = 114.4° \pm 3.8°$) with a contact angle hysteresis of ~10° for the advancing and receding, identifying that this SAM is the most hydrophobic. The surface with the highest hysteresis was the Au interface. The literature suggests that gold can be easily contaminated with physiosorbed species resulting in contamination on its surface [10] and occurs rapidly (~mins) once the clean surface is exposed to the ambient[21]. The SAM layers seem to have reduced hysteresis on the surface of the gold by adding a monolayer that reduces the tendency to adsorb hydrocarbons to the surface.

Figure 7b illustrates the energy profiles of both SAMs and the bare gold surface. The presence of the SAMs results in a reduction of the interfacial energy of the gold surface (~45 mJ/m^2). As expected, PFDT causes the most dramatic drop in energy due to the presence of the fluorinated groups [22]. This is indicative in **Figure 7** as the 1DT (CH_3 terminated) is still much higher in energy ~33 mJ/m^2 , in relation to the CF_3 terminated PFDT (~10mJ/m^2).

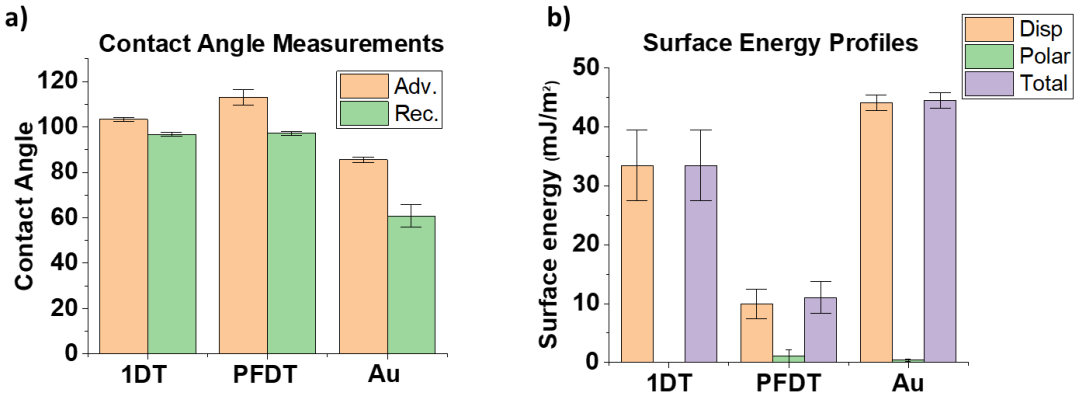

Figure 7 (a) Contact angle measurements for advancing and receding behaviour of H_20 for 1-decanethiol (1DT), 1H,1H,2H,2H-Perfluorodecanethiol (PFDT) and gold (Au) **(b)** Surface energy profile using the Fowkes approach [13], [14] to determine the surface energies of 1-decanethiol (1DT), 1H,1H,2H,2H-Perfluorodecanethiol (PFDT) and gold (Au). This was calculated using advancing CA of water and diiodomethane.

3.2 Surface roughness measurements

Surface roughness was also measured using AFM as shown in Figure 8 for 5 x 5 µm and 1x1 µm scan areas. The scans performed at over larger areas confirmed that the surfaces were uniform at length scales comparable to the FDTR probe spot size. Moreover, root-mean-square (RMS) surface roughness measurements showed that in all cases the surfaces were exceptionally smooth and showed no signs of gross defects that could interfere with the FDTR measurements. The smoothest surface was found to be PFDT with an RMS values of 0.3 nm. Since roughness can contribute to the interpretation of the measured contact angles [23], we quantified the roughness factor (RF) of each sample using the small area scans. We found RF ≈ 1 for all surface types; ruling out significant roughness effects on the surface energy contributions subsequently inferred from the contact angle measurements.

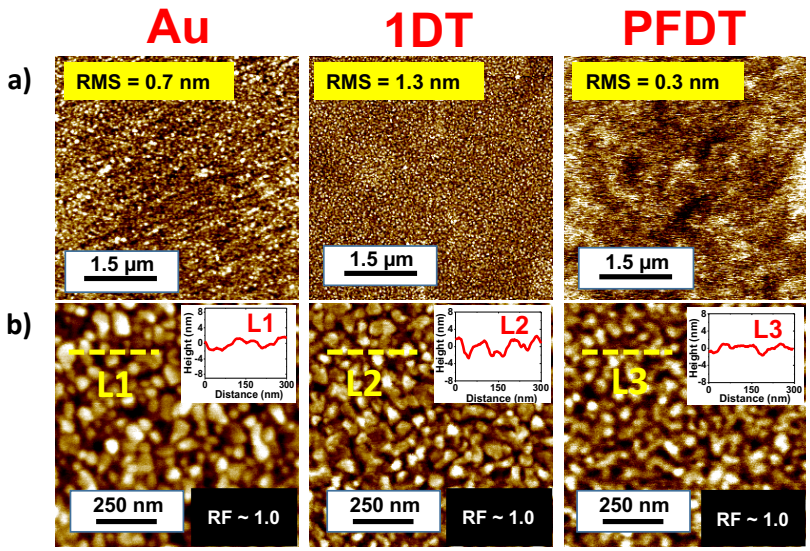

Figure 8. AFM images of (a) 5 x 5 µm (b) 1 x 1 µm of gold, 1-decanethiol (1DT), 1H,1H,2H,2H-Perfluorodecanethiol (PFDT)

3.3 FDTR phase lag measurements and fittings

We measured the phase lag of each cell setup for each testing fluids with bare Au, 1DT and PFDT surfaces. κ and G of each cell were determined by taking the average of three independent measurements at different sites on the sample surface as shown in Figure 9. Images captured with CCD_2 were used to avoid regions on the sample surface demonstrating obvious defects and particulate contamination.

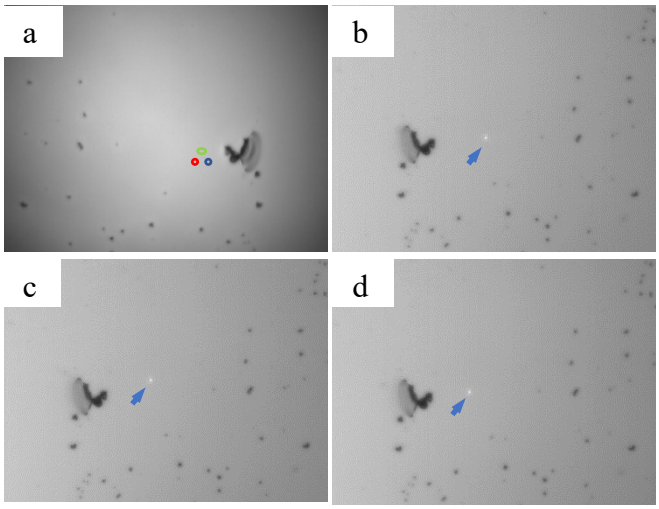

Figure 9: Transducer surface of a deionised water cell observed from (a) CCD 1 and indication of the locations of three sites measured in red, green and blue, respectively. Surfaces in (b), (c) and (d) were observed through CCD 2, where the overlapped pump and probe spots can be seen from CCD 2 via transmission

For more accurate measurement of κ and G, we independently measured the thermal conductivity of the glass substrate (~1.3 $Wm^{-1}K^{-1}$) and kept this value constant in all subsequent fittings [4]. Our fitting approach allowed κ and G to vary while allowing bulk liquid volumetric heat capacity to vary by ±1% of the known value. We fitted ethanol data and determined κ and G simultaneously (see Figure 10). Our measured κ agrees with to literature, and this provides confidence in our G value of 2.09 ± 0.1 $MWm^{-2}K^{-1}$ on bare Au (see **Table 1**). With the treated Au surfaces, we observed ~30% and ~35% increase in G for 1DT and PFDT SAMs, respectively. We also measured deionised water and saw increase in G with 1DT and PFDT SAM surfaces in comparison the bare Au surface (see **Table 2**). Although we see a significant improvement with the SAM layer at the interface, we should only consider the differences as relative changes and not take the of G at face value due to batch-to-batch surface preparation and surface roughness variations. Indeed, Acharya *et al.* have shown that surface roughness, in the form of varying SAM molecular lengths, can influence G significantly [5].

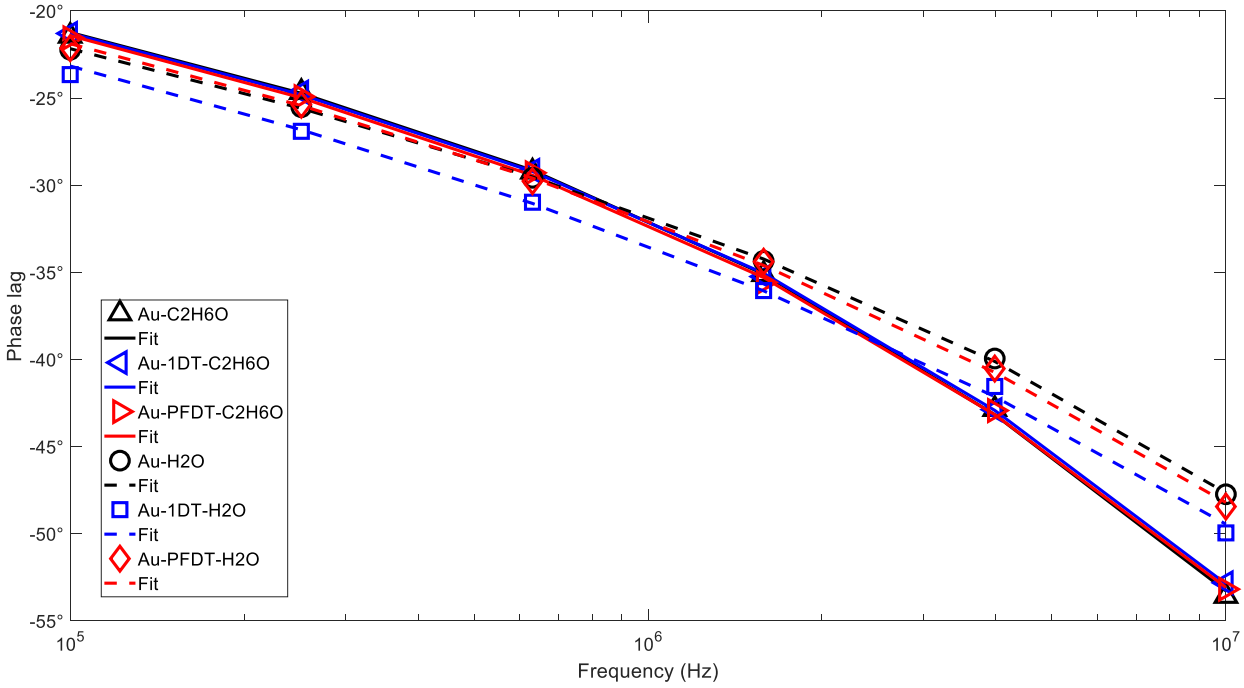

Figure 10: Measured phase lag as a function of frequency for ethanol and water on the bare Au, 1DT SAM and PFDT SAM surfaces. Data and best fits are represented by markers and lines, respectively.

	κ_{C2H6O} ($Wm^{-1}K^{-1}$)	G ($MWm^{-2}K^{-1}$)	Expected κ at 300 K [24]
Au-C2H6O	0.172 ± 0.008	2.09 ± 0.2	0.171
Au-1DT-C2H6O	0.162 ± 0.02	2.71 ± 0.16	
Au-PFDT-C2H6O	0.168 ± 0.02	2.81 ± 0.02	

Table 1: Measured κ and G for ethanol in contact with bare Au, 1DT and PFDT.

Figure 11 compares our G measurements for ethanol to the only other dataset available for ethanol/SAM interfaces [4]. We observe that, in comparison, our ethanol/bare Au G is ~8.5x smaller. Moreover, both SAMs measured here demonstrate more than an order of magnitude smaller G in comparison to the measurements of Tian *et al.* despite the similarity of the SAMs studied, e.g., nature of the ligand bond. Moreover, we can rule out the slight difference in the SAM molecule carbon chain length. As such, the current cause of the inconsistency remains unresolved.

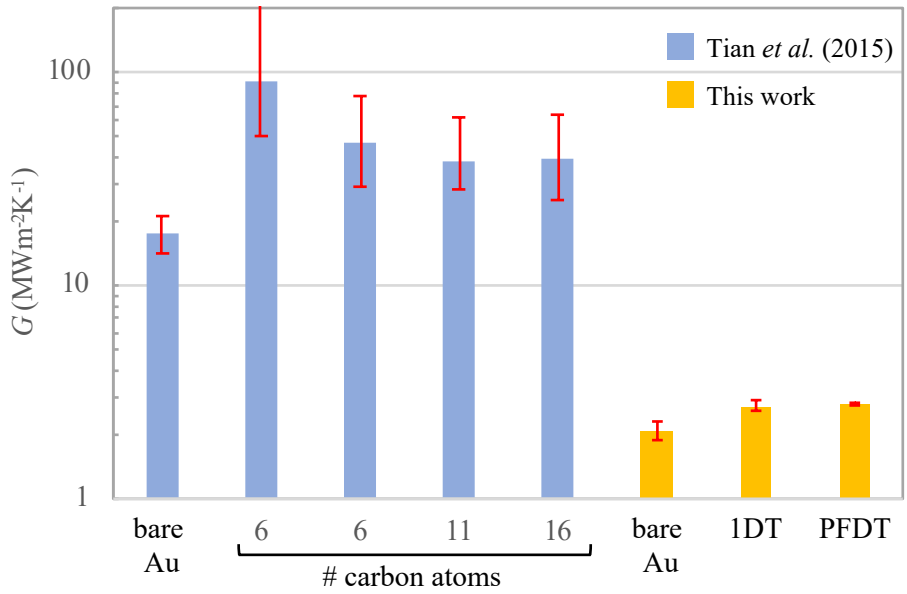

Figure 11: Interface conductance G of ethanol measured by Tian *et al.* [4] for hydrogenated SAMs on Au and in this work.

	κ_{H2O} (Wm^{-1}K^{-1})	G (MWm^{-2}K^{-1})	Expected κ at 300 K [24]
Au-H2O	0.565 ± 0.074	32.88 ± 2.6	0.609
Au-1DT-H2O	0.6 ± 0.028	60.27 ± 11.6	
Au-PFDT-H2O	0.608 ± 0.028	74.45 ± 6.86	

Table 2: Measured κ and G for deionised water in contact with bare Au, 1DT and PFDT.

Figure 12 shows our measured G for water as a function of the dimensionless work of adhesion, $1+\cos(\theta_a)$, in comparison to previous experimental and simulation studies in the literature. Our measured value of G for 1DT at $1+\cos(\theta_a) \sim 0.75$ is consistent with the value found by Ge *et al.* for a similar hydrocarbon chain [2]. However, our data for PFDT at $1+\cos(\theta_a) \sim 0.59$ is more consistent with the trendline fitted to the data of Harikrishna *et al.* [3]. Moreover, based on all previous results shown here, both simulation and experimental, we expect G to scale proportionally with work of adhesion, $G \propto 1+\cos(\theta_a)$. However, for our measurements, we observe the opposite trend. More investigation is required to resolve this apparent inconsistency.

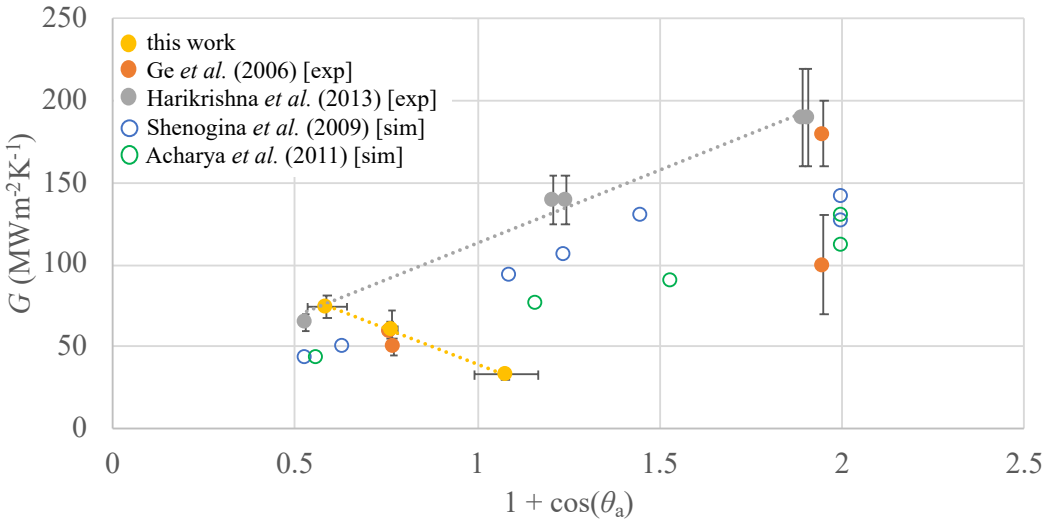

Figure 12: Interface conductance G of water as a function of the dimensionless work of adhesion for this work and from the literature [2], [3], [5], [6]. The grey dashed line is a linear fit to the data of Harikrishna *et al.* [3]. The yellow dashed line is a linear fit to the data measured in this work.

For Galden HT80, we fitted (see **Figure 13**(a)) and determined $\kappa \sim 0.063$ $Wm^{-1}K^{-1}$ and $G \sim 0.244$ $MWm^{-2}K^{-1}$ on bare Au. Our measured κ is consistent with the expected value [25]. However, we found that it was not possible to distinguish differences in G between the bare Au, 1DT and PFDT SAM surfaces. We briefly turned to qualitative observations regarding the goodness of fit. To see how the modelled value of G effected the goodness of fit, we artificially inflated G and generated various phase lag profiles. Even at ten times G, such profiles could arguably be considered a relatively good fit to measured data (see **Figure 13**b) indicating poor sensitivity of the measurement to that parameter.

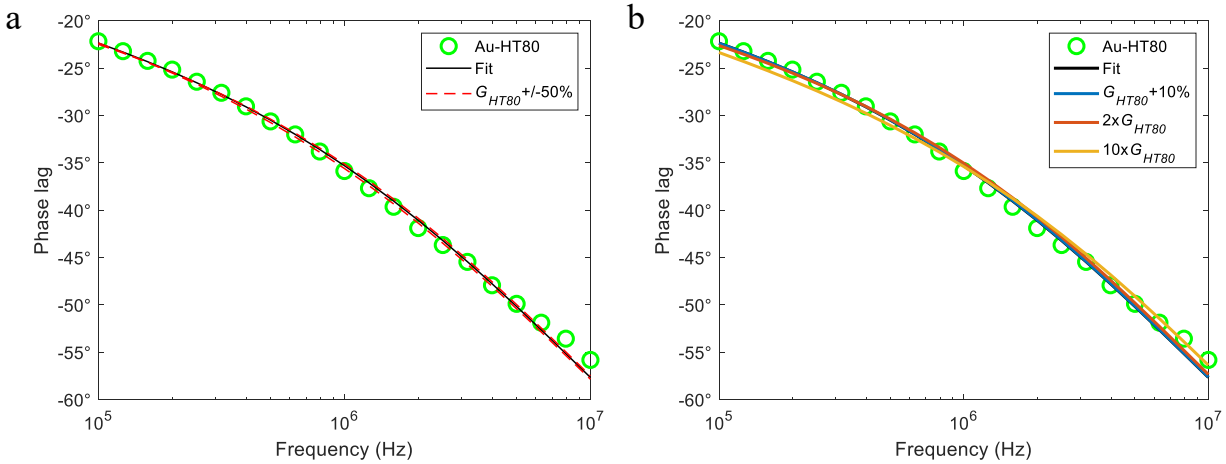

Figure 13: Fitting G for Galden HT80. (a) Data for the bare Au surface showing best fit and ±50% variation in best fitted G. (b) Data for the bare Au surface showing best fit and +10%, +200% and +1000% variation in best fitted G.

To understand the poor sensitivity of the FDTR measurements with Galden HT80, we compared the frequency-dependent sensitivities of the three tested liquids. **Figure 14** shows that better sensitivity to κ corresponds to larger values of κ and that this leads to better sensitivity for G. This can be understood by recognizing the bidirectional nature of heat flow in our system. For the sensor substrate employed here, heat flow from Au transducer layer towards the glass substrate ($\kappa_{glass} \approx 1.3$ $Wm^{-1}K^{-1}$) was always favored for each of the tested liquids, but this adverse heat flow was most pronounced for measurements involving Galden HT80 with its thermal conductivity ~20× smaller than the glass substrate. This underscores the need for a

carefully designed sensor substrate in order to improve the sensitivity and significance of measurements involving low conductivity liquids such as fluorinated refrigerants.

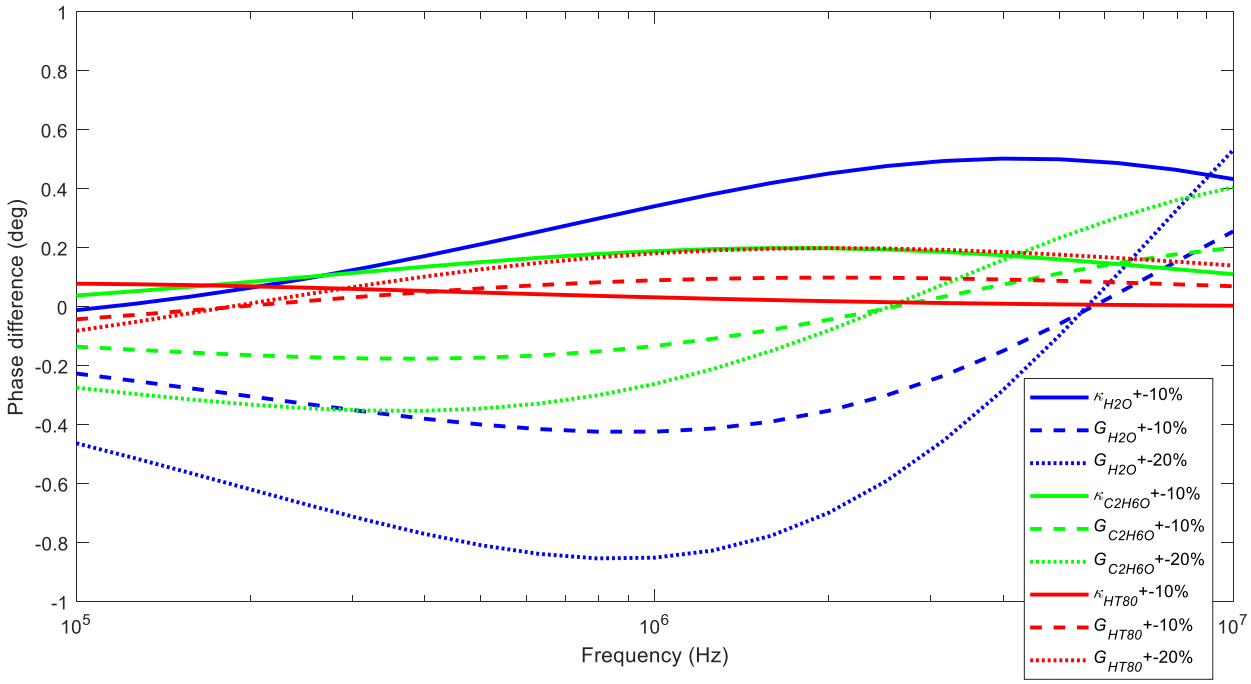

Figure 14: Sensitivity analysis of the κ and G fittings for the three tested liquids. Phase differences were calculated by keeping all parameters constant except for κ and take the difference of $\kappa + 10\%$ estimated phase lag with $\kappa - 10\%$, and similarly for G.

4. CONCLUSIONS

The effect of self-assembled monolayers on the thermal interface conductance (G) of ethanol, water and a model dielectric heat transfer fluid, Galden HT80 were assessed using a combination of surface characterization (contact angle goniometry, AFM) and frequency domain thermoreflectance (FDTR) measurements.

Contact angle measurements using two probe liquids, water and diiodomethane, were used to assess the surface energy contributions of the tested surfaces. AFM measurements revealed that the tested surfaces were smooth and free of defects at length scales comparable to the FDTR probe laser.

Using FDTR, thermal conductivity κ was measured for the working fluids deionised water, ethanol and Galden HT80 and interfacial conductance G in contact with bare Au, 1DT and PFDT surfaces. The presence of a SAM layer had a weak, but measurable effect on G for ethanol. However, absolute values were significantly lower than ones measured previously using TDTR. The SAM layer had a strong effect on water similar to previous findings. However, we found that, contrary to the expected behavior, G increased with increasing advancing contact angle. This needs to be further investigated in the context of our measurement protocols. We were unable to distinguish interfacial thermal conductance differences between HT80 and bare Au, 1DT and PFDT, respectively. Due to the low thermal conductivity of Galden HT80 and the limited sensitivity afforded to us by our current FDTR surface sensor design, we were unable to make a significant determination of G. This remains an outstanding challenge and the focus of future work.

ACKNOWLEDGEMENTS

P.D. and K.Y. would like to thank Irish Research Council for funding under grants EBPPG/2018/255 and EBPPG/2018/265.

REFERENCES AND CITATIONS

[1] D. F. Hanks *et al.*, "Nanoporous membrane device for ultra high heat flux thermal management," *Microsyst. Nanoeng.*, 2018.
[2] Z. Ge, D. G. Cahill, and P. V. Braun, "Thermal conductance of hydrophilic and hydrophobic interfaces," *Phys. Rev. Lett.*, 2006.
[3] H. Harikrishna, W. A. Ducker, and S. T. Huxtable, "The influence of interface bonding on thermal transport through solid-liquid interfaces," *Appl. Phys. Lett.*, vol. 102, no. 25, Jun. 2013.
[4] Z. Tian, A. Marconnet, and G. Chen, "Enhancing solid-liquid interface thermal transport using self-assembled monolayers," *Appl. Phys. Lett.*, 2015.
[5] H. Acharya, N. J. Mozdzierz, P. Keblinski, and S. Garde, "How Chemistry, Nanoscale Roughness, and the Direction of Heat Flow Affect Thermal Conductance of Solid–Water Interfaces," *Ind. Eng. Chem. Res.*, vol. 51, no. 4, pp. 1767–1773, Feb. 2012.
[6] N. Shenogina, R. Godawat, P. Keblinski, and S. Garde, "How Wetting and Adhesion Affect Thermal Conductance of a Range of Hydrophobic to Hydrophilic Aqueous Interfaces," *Phys. Rev. Lett.*, vol. 102, no. 15, p. 156101, Apr. 2009.
[7] C. D. Bain, E. B. Troughton, Y. T. Tao, J. Evall, G. M. Whitesides, and R. G. Nuzzo, "Formation of Monolayer Films by the Spontaneous Assembly of Organic Thiols from Solution onto Gold," *J. Am. Chem. Soc.*, 1989.
[8] A. J. Schmidt, R. Cheaito, and M. Chiesa, "A frequency-domain thermoreflectance method for the characterization of thermal properties," *Rev. Sci. Instrum.*, 2009.
[9] D. O'Hagan, "Understanding organofluorine chemistry. An introduction to the C-F bond," *Chem. Soc. Rev.*, 2008.
[10] E. G. Shafrin and W. A. Zisman, "Effect of progressive fluorination of a fatty acid on the wettability of its adsorbed monolayer," *J. Phys. Chem.*, 1962.
[11] R. Colorado and T. R. Lee, "Thiol-based Self-assembled Monolayers: Formation and Organization," in *Encyclopedia of Materials: Science and Technology*, 2001.
[12] M. Zenkiewicz, "Methods for the calculation of surface free energy of solids," *J. Achiev. Mater. Manuf. Eng.*, 2007.
[13] F. M. Fowkes, "Attractive forces at interfaces," *Ind. Eng. Chem.*, vol. 56, no. 12, pp. 40–52, Dec. 1964.
[14] R. Lundy *et al.*, "Exploring the Role of Adsorption and Surface State on the Hydrophobicity of Rare Earth Oxides," *ACS Appl. Mater. Interfaces*, vol. 9, no. 15, pp. 13751–13760, 2017.
[15] J. Zhu, D. Tang, W. Wang, J. Liu, K. W. Holub, and R. Yang, "Ultrafast thermoreflectance techniques for measuring thermal conductivity and interface thermal conductance of thin films," *J. Appl. Phys.*, 2010.
[16] K. Yu, P. Darragh, N. K. Balla, R. Enright, and D. McCloskey, "'Thermal Measurements at solid-liquid interfaces transporting high heat fluxes using frequency domain thermoreflectance,'" *Proc. 14th Int. Conf. Heat Transf. Fluid Mech. Thermodyn. HEFAT Wicklow 2019*, 2019.
[17] A. Schmidt, M. Chiesa, X. Chen, and G. Chen, "An optical pump-probe technique for measuring the thermal conductivity of liquids," *Rev. Sci. Instrum.*, 2008.
[18] H. S. Carslaw and J. C. Jaeger, "Conduction of heat in solids," *Oxf. Clarendon Press 1959 2nd Ed*, 1959.
[19] C. A. Schneider, W. S. Rasband, and K. W. Eliceiri, "NIH Image to ImageJ: 25 years of image analysis," *Nat. Methods*, vol. 9, pp. 671–675, 2012.
[20] R. Raj, R. Enright, Y. Zhu, S. Adera, and E. N. Wang, "Unified Model for Contact Angle Hysteresis on Heterogeneous and Superhydrophobic Surfaces," *Langmuir*, vol. 28, no. 45, pp. 15777–15788, Oct. 2012.

[21] D. J. Preston, N. Miljkovic, J. Sack, R. Enright, J. Queeney, and E. N. Wang, "Effect of hydrocarbon adsorption on the wetting of rare earth oxides," in *Proceedings of the 15th International Heat Transfer Conference, IHTC 2014*, 2014.

[22] V. H. Dalvi and P. J. Rossky, "Molecular origins of fluorocarbon hydrophobicity," *Proc. Natl. Acad. Sci.*, vol. 107, no. 31, p. 13603, Aug. 2010.

[23] R. Wenzel, "Resistance of solid surfaces to wetting by water," *Ind Eng Chem*, vol. 28, no. 8, pp. 988–994, 1936.

[24] E. W. Lemmon, M. O. McLinden, and D. G. Friend, "Thermophysical properties of fluid systems," in *NIST Chemistry WebBook, NIST Standard Reference Database Number 69*, P. J. Linstrom and W. G. Mallard, Eds. National Institute of Standards and Technology, 2005.

[25] "Solvay Specialty Polymers Galden® HT80 PFPE Heat Transfer Fluid," *MatWeb*, 07-Oct-2019. [Online]. Available: www.matweb.com.